


Coexisting antiferromagnetic phases on the frustrated pyrochlore sublattice of the mixed Jahn-Teller system $\text{Ni}_{1-x}\text{Cu}_x\text{Cr}_2\text{O}_4$

M. Reehuis , M. Tovar, B. Klemke, D. M. Többens, A. Hoser, and J.-U. Hoffmann
Helmholtz-Zentrum Berlin für Materialien und Energie, D-14109 Berlin, Germany



(Received 13 March 2024; accepted 8 May 2024; published 21 May 2024)

The magnetic order and phase transitions in the normal spinel system $\text{Ni}_{1-x}\text{Cu}_x\text{Cr}_2\text{O}_4$ are studied by powder-neutron and x-ray diffraction, as well as by magnetization measurements to get a complete magnetic phase diagram. For chromites with $x(\text{Cu}) > 0.5$ a canted antiferromagnetic phase of Cr appears first, followed by the onset of ferromagnetism in the Cu sublattice at lower temperature forming a ferrimagnetic lattice. Conversely, with $x(\text{Cu}) < 0.5$ the ferrimagnetic order between the Cr and Cu spins occurs at the higher ordering temperature followed by the onset of antiferromagnetic order in the Cr sublattice. Apart from the crossing of the two boundary lines of the transition temperatures at $x(\text{Cu}) = 0.50$ a compensation point of the ferrimagnetic moments is determined at $x(\text{Cu}) = 0.60$, where the spontaneous magnetization has almost completely vanished. Most remarkable is the antiferromagnetic Cr ordering on the orthorhombic distorted pyrochlore lattice for samples in the $x(\text{Cu})$ range from 0 to 0.12 due to the large variety of coexisting magnetic phases. In the magnetic ground state of NiCr_2O_4 two commensurate antiferromagnetic structures with the propagation vectors $\mathbf{k}_{\text{AF}} = (0,0,1)$ and $(\frac{1}{2},\frac{1}{2},\frac{1}{2})$ coexist. With increasing Cu content from $x(\text{Cu}) = 0$ to 0.09 these phases undergo a transition to another commensurate structure with $\mathbf{k} = 0$ via two coexisting incommensurate magnetic phases with the vectors $\mathbf{k}_{\text{IC1}} = (0,0,k_z)$ and $\mathbf{k}_{\text{IC2}} = (0,k_y,k_z)$. The different magnetic phases are discussed qualitatively based on the lattice dimensions depending on the concentration ratio of two Jahn-Teller ions at the tetrahedral *A* site, where Ni^{2+} causes elongated and Cu^{2+} compressed tetragonal lattice distortions. Further, magnetoelasticity studies on selected samples indicate that the magnetically induced lattice strains follow the symmetry of the underlying Jahn-Teller distorted lattices.

DOI: [10.1103/PhysRevMaterials.8.054414](https://doi.org/10.1103/PhysRevMaterials.8.054414)

I. INTRODUCTION

The pyrochlore lattice of corner-connected tetrahedra is a prominent structure to be geometrically frustrated for systems with antiferromagnetic spin coupling [1,2]. In spinels with the general formula AB_2O_4 the *B*-site atoms form a pyrochlore lattice [3]. In chromites, where *A* is a divalent nonmagnetic cation (Mg^{2+} , Zn^{2+} , Cd^{2+} , or Hg^{2+}), the magnetic Cr^{3+} ion at the *B* site is in the $3d^3$ configuration in which the t_{2g} levels are half filled [4]. Therefore, the Cr^{3+} ion is not Jahn-Teller active and cooperative distortions of the CrO_6 octahedra cannot be induced. For not too large distances between nearest-neighbor Cr^{3+} ions the magnetic coupling is antiferromagnetic and magnetic frustration becomes relevant for magnetic ordering [4]. Frustration means that not all six antiparallel couplings can be satisfied simultaneously on a regular tetrahedron. A measure of the level of frustration is the antiferromagnetic ordering temperature T_N as compared to a transition temperature Θ that is derived from a Curie-Weiss analysis. The magnetic behavior of ZnCr_2O_4 with a frustration index $f = \Theta/T_N$ of about 30 is a well-known example [5]. Inherent to frustration at low temperature is a macroscopic degeneracy of magnetic structures or ultimately the absence of order [6].

In NiCr_2O_4 and CuCr_2O_4 the magnetic Ni^{2+} and Cu^{2+} ions have theoretical spin-only moments $\mu_S = 2 \cdot S = 2 \mu_B$ (Ni^{2+}) and $1 \mu_B$ (Cu^{2+}). These ions are located at the tetrahedral *A* site (Fig. 1) and ferrimagnetically coupled with the *B*-site

ions as found in many other spinels [7]. It was shown that the ferrimagnetic coupling sets in concomitantly with the structural phase transition from the tetragonal phase with the space group $I4_1/amd$ to the orthorhombic one with $Fddd$ [8–10]. Of particular importance are opposing Jahn-Teller (JT) distortions leading to a stretching of the NiO_4 and a compression of the CuO_4 tetrahedra [10,11]. As shown in Ref. [12], in a compressed tetragonal lattice (in our case CuCr_2O_4) a uniaxial magnetic structure with strong antiferromagnetic bonds is present for four Cr-Cr pairs with short distances in a Cr_4 tetrahedron of the pyrochlore lattice, and a ferromagnetic spin alignment is found for the remaining two pairs with larger distance. Conversely, a stretched tetragonal lattice (in our case NiCr_2O_4) has two strong and four weaker couplings (Fig. 1). The degree of tetragonal distortions lowers the degeneracy of possible magnetic structures as compared to cubic systems. Indicated by the observed antiferromagnetic ordering temperatures for the frustrated Cr sublattice, extensive degeneracy persists for NiCr_2O_4 , whereas frustration effects become negligible for CuCr_2O_4 . Besides the unusual structural and magnetic properties of chromium spinels it was reported that CuCr_2O_4 was identified as a multiferroic material, where ferroelectric order occurs well above the magnetic phase transition temperatures [13]. It is worth mentioning that CoCr_2O_4 is also a multiferroic material [14].

Due to the interesting structural and physical properties of NiCr_2O_4 and CuCr_2O_4 , research activities were extended

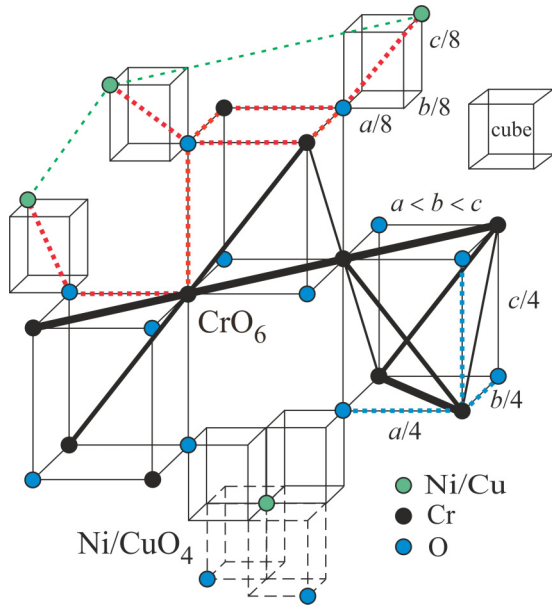


FIG. 1. Orthorhombic distortions in the $\text{Ni}_{1-x}\text{Cu}_x\text{Cr}_2\text{O}_4$ lattice. Black lines mark direct exchanges between nearest-neighbor Cr^{3+} ions, where the line thickness indicates the bond strength. Dashed blue and red lines indicate superexchange pathways via oxygen ions between the nearest Cr^{3+} ions and between the nearest-neighbor Cr^{3+} and $\text{Ni}^{2+}/\text{Cu}^{2+}$ ions. Thin green dashed lines connect nearest-neighbor $\text{Ni}^{2+}/\text{Cu}^{2+}$ ions. Possibly weak superexchange interactions exist in $\text{Ni}/\text{Cu}-\text{O}-\text{O}-\text{Ni}/\text{Cu}$ and $\text{Ni}/\text{Cu}-\text{O}-\text{Cr}-\text{O}-\text{Ni}/\text{Cu}$. The Cr_4 tetrahedra are embedded by cuboid cells with an edge length of a one-quarter of the crystallographic unit cell. Smaller cuboid cells with edge lengths of one-eighth of the unit cell have a $\text{Ni}/\text{Cu}-\text{O}$ pair along the diagonal. Four of these cells with common $\text{Ni}^{2+}/\text{Cu}^{2+}$ ions in the center indicate the distorted tetrahedral oxygen coordination $(\text{Ni}/\text{Cu})\text{O}_4$ (bottom). The position of the CrO_6 octahedron is marked as well.

by further investigations on mixed systems, where the A -site atoms were replaced by divalent magnetic or nonmagnetic metal ions. In the frustrated system $\text{Ni}_{1-x}\text{Mg}_x\text{Cr}_2\text{O}_4$ an increasing Mg^{2+} content causes a continuous reduction of the ferri- and antiferromagnetic transition temperatures and goes to a spin-glass-like state [15]. An increasing Mg^{2+} content in the system $\text{Cu}_{1-x}\text{Mg}_x\text{Cr}_2\text{O}_4$ leads to a melting of cooperative Jahn-Teller distortions which are correlated with rather strong tetragonal distortions [16]. Here, the change of lattice parameters could be described formally in terms of macroscopic strains. To elucidate the origin of ferroelectricity, observed earlier in CuCr_2O_4 [14], a detailed study of the structural, electrical, and magnetic properties was carried out on the mixed system $\text{Cu}_{1-x}\text{Mg}_x\text{Cr}_2\text{O}_4$ [17]. In another study on the mixed system $\text{Cu}_{1-x}\text{Co}_x\text{Cr}_2\text{O}_4$ the interplay between Jahn-Teller distortion-driven orbital order and the structural instability correlated with the occurrence of ferroelectric order was investigated [14]. Here, the Co^{2+} ion in the electronic d^7 configuration is not Jahn-Teller active at the tetrahedral A site. On the other hand, a ferrimagnetic coupling sets in between the magnetic ions Co^{2+} and Cr^{3+} around 95 K [18,19].

A systematic x-ray- and neutron-diffraction study carried out earlier [20] provided insight into the interplay between

the Jahn-Teller effect, geometrical frustration, and long-range magnetic order in the mixed system $\text{Ni}_{1-x}\text{Cu}_x\text{Cr}_2\text{O}_4$. Recently published data on NiCr_2O_4 and the mixed chromite $\text{Ni}_{0.98}\text{Cu}_{0.02}\text{Cr}_2\text{O}_4$ revealed the existence of new commensurate and incommensurate magnetic phases [21]. The coexistence of different phases and their observed exceptional temperature dependencies should be emphasized. On the Cu-rich side a spin reorientation was identified between $x(\text{Cu}) = 0.90$ and 1 [22]. Analyses of magnetic powder-diffraction patterns of CuCr_2O_4 revealed a symmetric spin coupling of the Cr_{AF} and Cr_{F} modes for the canted antiferromagnetic Cr spin structure [13]. High-resolution x-ray-diffraction studies of NiCr_2O_4 and CuCr_2O_4 are certainly worth mentioning since the observation of magnetoelastic strains around magnetic phase transitions provides insights into magnetic exchanges [10].

These studies reveal the existence of a complex magnetic phase diagram of the system $\text{Ni}_{1-x}\text{Cu}_x\text{Cr}_2\text{O}_4$. In the present work we therefore extend investigations on the entire range of this system. We especially focus on the Ni-rich mixed chromites from $x(\text{Cu}) = 0$ to 0.15, where one finds a complex antiferromagnetic order in the Cr sublattice. Additional high-quality powder samples were investigated by x-ray- and neutron diffraction to determine the T and $x(\text{Cu})$ dependence of magnetic ordering as well as to explore the onset of magnetoelasticity. Supplementary magnetization measurements were performed to study directly the ferro- or ferrimagnetic behavior and the onset of magnetic phase transitions.

II. EXPERIMENTAL DETAILS

For the present study we used the same samples of the system $\text{Ni}_{1-x}\text{Cu}_x\text{Cr}_2\text{O}_4$ which were prepared earlier by the precursor method in steps of $\Delta x(\text{Cu}) = 0.10$ and two more samples with $x(\text{Cu}) = 0.75$ and 0.95 [20]. Our investigations revealed that various magnetic changes appear in the range between $x(\text{Cu}) = 0$ and 0.12. Therefore, in this range more samples were prepared in smaller steps of $\Delta x(\text{Cu}) = 0.02$ and another one with $x(\text{Cu}) = 0.09$. All powder samples were reannealed at 1200 K for 5–7 days to minimize internal stress, achieving a high degree of homogeneity. An estimation of concentration inhomogeneities is briefly outlined in the following Sec. III. For this analysis temperature-dependent x-ray-diffraction studies were performed at the Helmholtz-Zentrum Berlin (HZB) on the laboratory Guinier diffractometer Huber 645 and on the KMC2 diffractometer at the BESSY synchrotron [23], where the latter is equipped with a modified Gifford-McMahon closed-cycle cryocooler TMP-CCR HXR [24]. On both instruments the wavelength 1.5406 Å was used.

Neutron-diffraction studies were carried out on the powder diffractometers E2 and E6 using the wavelengths 2.38 and 2.43 Å. Further details are given elsewhere [20,21,25]. The FULLPROF suite was used for profile refinements of powder patterns and for simulating patterns for different magnetic structural models. The routines k -search and *BasIreps* were used to determine magnetic wave vectors and basis vectors for the symmetry-allowed magnetic structures [26]. A Physical Properties Measurement System (PPMS, Quantum Design, operated by the CoreLab Quantum Measurements at HZB)

was used for magnetization measurements. Magnetization curves were measured at temperatures from 5 to 300 K in applied magnetic fields up to 14 T.

III. RESULTS AND DATA ANALYSIS

A. Sample quality

Since sample homogeneity is of essential importance for the precise determination of a phase diagram, an estimation of concentration inhomogeneities is briefly outlined in the following. Changes of the magnitude of moments in a magnetically ordered state are accompanied by a change of lattice constants due to magnetoelastic coupling. This is most pronounced at a phase transition, where the magnetization changes sharply. For samples of the system $\text{Ni}_{1-x}\text{Cu}_x\text{Cr}_2\text{O}_4$ with small differences in $x(\text{Cu})$ and magnetic ordering temperatures T_{AF} , a maximum of the difference between the lattice constants, in our case Δa , occurs precisely between the two ordering temperatures. A single-peak analysis of the 400 reflection of $\text{Ni}_{0.85}\text{Cu}_{0.15}\text{Cr}_2\text{O}_4$ and $\text{Ni}_{0.82}\text{Cu}_{0.18}\text{Cr}_2\text{O}_4$ around their magnetic transitions at $T_{\text{AF}} = 46$ K and $T_{\text{AF}} = 52$ K shows that $\Delta a = a_{\text{Ni}_{0.85}} - a_{\text{Ni}_{0.82}}$ is about 0.015 Å between 30 and 40 K. It increases up to a maximum value of 0.03 Å at 48 K and then decreases again to 0.019 Å at 56 K. Above 40 K the magnetoelastic expansion of $a_{\text{Ni}_{85}}$ begins first and Δa increases with increasing AF order around $T_{\text{AF}} = 46$ K. A similar increase at higher temperature occurs for $a_{\text{Ni}_{82}}$ around 52 K and causes a reduction of Δa . This explains the peak maximum in Δa at about 48 K. A similar temperature behavior is observed for the linewidth of $\text{Ni}_{0.82}\text{Cu}_{0.18}\text{Cr}_2\text{O}_4$ with an additional line broadening of about 30% compared to the linewidth outside the “magnetoelastic” transition. The line broadening is determined by the concentration gradient of the sample. Scaling to the measured Δa for the $\text{Ni}_{0.82}/\text{Ni}_{0.85}$ ratio gives an inhomogeneity of about 0.002–0.004 for $\text{Ni}_{0.82}\text{Cu}_{0.18}\text{Cr}_2\text{O}_4$. The estimated small inhomogeneity is confirmed by the observations for $\text{Ni}_{0.91}\text{Cu}_{0.09}\text{Cr}_2\text{O}_4$, where the magnetic phase with $\mathbf{k} = 0$ is present and the incommensurate one with $\mathbf{k} = (0,0,k_z)$ is absent, and conversely for $\text{Ni}_{0.92}\text{Cu}_{0.08}\text{Cr}_2\text{O}_4$, where the phase with $\mathbf{k} = (0,0,k_z)$ is present and the other one with $\mathbf{k} = 0$ is absent (see below).

B. Magnetic phase transitions

To investigate the onset of long-range magnetic ordering we have performed x-ray- and neutron-diffraction experiments as well as PPMS measurements on several samples of the system $\text{Ni}_{1-x}\text{Cu}_x\text{Cr}_2\text{O}_4$ covering the entire concentration range. Neutron-powder diffraction was used for the detection of magnetic phase transitions, where magnetic intensity spontaneously appears at the position of Bragg reflections generated by the rule $(hkl)_{\text{M}} = (hkl)_{\text{N}} \pm \mathbf{k}$. Different coexisting magnetic phases could be distinguished by their propagation vectors \mathbf{k} . Further evidence of magnetic phase transitions are spontaneous lattice distortions due to magnetoelastic effects as investigated by x-ray- and neutron-diffraction data. Additionally, magnetization measurements were performed in a weak field of 0.05 T, where

magnetic phase transitions become visible through spontaneous changes in the curvature of $M(T)$.

To give an overview of the magnetic properties of this spinel system, four characteristic $M(T)$ curves are shown in Fig. 2. For $\text{Ni}_{0.70}\text{Cu}_{0.30}\text{Cr}_2\text{O}_4$, representing a Ni-rich mixed chromite, the appearance of ferrimagnetic ordering is evident by a sudden increase in $M(T)$. Here, the difference between the antiparallel coupled magnetic moments of the Ni/Cu and Cr sublattices results in a net magnetization. The inflection point marks the ferrimagnetic transition temperature T_{FI} that is the highest magnetic ordering temperature in this sample [Fig. 2(d)]. It should be noted that all determined transition temperatures obtained from PPMS measurements show a good agreement with those obtained from neutron powder-diffraction data. Further cooling leads to a flattening of $M(T)$ which is typical for ferro- or ferrimagnets. However, the $M(T)$ curve in Fig. 2(d) shows an anomaly at 81 K, where a weak spontaneous increase of magnetization appears. Our neutron data revealed that this transition can be attributed to the onset of the additional AF1 ordering in the Cr sublattice with the propagation vector $\mathbf{k}_{\text{AF1}} = 0$.

For $\text{Ni}_{0.30}\text{Cu}_{0.70}\text{Cr}_2\text{O}_4$, representing a Cu-rich mixed chromite, such anomaly is not observable in the magnetization curve presented in Fig. 2(a). The overall behavior of $M(T)$ is similar to the curve of the end member CuCr_2O_4 , where the Cr^{3+} ions order first into a canted antiferromagnetic structure with a ferromagnetic (F) component tilted by about 24° to the AF component [12]. The F moment causes a relatively weak spontaneous magnetization M_0 , where the onset of F ordering in $\text{Ni}_{0.30}\text{Cu}_{0.70}\text{Cr}_2\text{O}_4$ is better visible at 124 K in the enlarged $M(T)$ curve of Fig. 2(a). Long-range ferromagnetic ordering of Ni/Cu starts at the lower temperature 113 K, where an antiparallel coupling of the Ni/Cu-F and Cr-F sublattices generates ferrimagnetism indicated by an inflection point in $M(T)$ curve. This behavior was observed for all samples between $x(\text{Cu}) = 0.60$ and 1, although the transition temperatures of both the canted AF (Cr-AF, Cr-F) and the additional F order (Ni/Cu-F) increase continuously with increasing Cu content as shown in Fig. 3.

The compensation point with an almost vanishing net magnetization is reached for $\text{Ni}_{0.40}\text{Cu}_{0.60}\text{Cr}_2\text{O}_4$ [Fig. 2(b)]. The increasing Ni content enlarges the average A-site moment, since the magnetic moment of Ni^{2+} is larger than that of Cu^{2+} . Up to $x(\text{Cu}) = 0.60$ the A-site moment almost compensates the antiparallel coupled moment of the Cr^{3+} ions at the B site. In Fig. 2(b), it is interesting to see that $M(T)$ decreases just below the order transition that behaves in a similar way as an antiferromagnet.

In $\text{Ni}_{0.50}\text{Cu}_{0.50}\text{Cr}_2\text{O}_4$ all three modes Cu-F, Cr-F, and Cr-AF line up practically at the same temperature and lead to a very steep rise in $M(T)$ as shown in Fig. 2(c). For samples with $x(\text{Cu}) < 0.50$ the Cr-AF order occurs below the ferrimagnetic transition temperature T_{FI} . It is noteworthy that the transition temperature of the ferromagnetic Cr-F mode is always the highest. All these results provide already valuable information to create a rich magnetic phase diagram for the entire concentration range of the mixed system $\text{Ni}_{1-x}\text{Cu}_x\text{Cr}_2\text{O}_4$, where the magnetic ordering temperatures are plotted versus $x(\text{Cu})$ in Fig. 3.

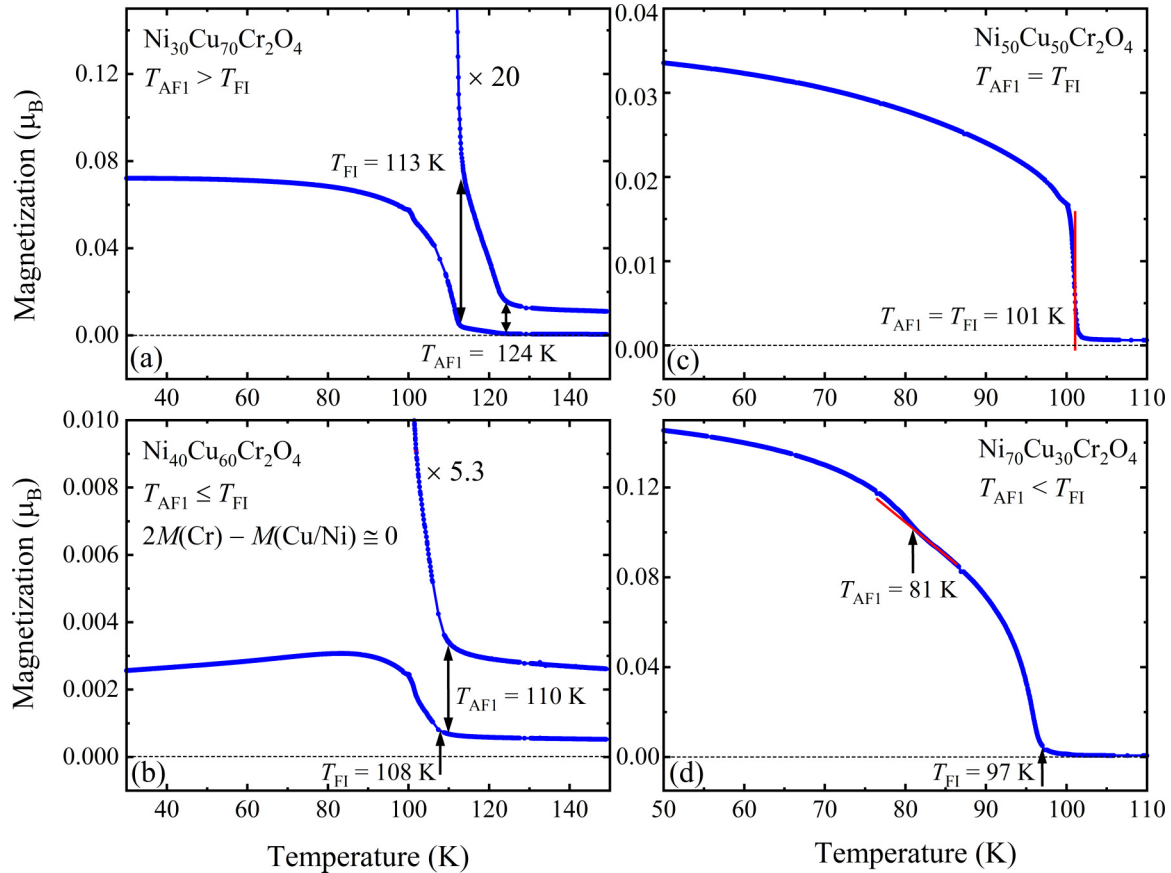


FIG. 2. Magnetization vs temperature for selected samples of $\text{Ni}_{1-x}\text{Cu}_x\text{Cr}_2\text{O}_4$ in an applied magnetic field of 0.05 T. Black arrows mark the AF1 and FI transition temperatures. (a) The AF1 phase in the Cu-rich chromite $\text{Ni}_{0.30}\text{Cu}_{0.70}\text{Cr}_2\text{O}_4$ is found to order above T_{FI} . The resulting ferromagnetic moments of the FI phase result in a strong increase of magnetization. At T_{AF} the AF ordering sets in concomitantly with the onset of an additional F ordering which is much weaker pronounced than in the FI phase. Therefore, the spontaneous increase of magnetization is only observable in the enlarged $M(T)$ curve shown above. (b) In $\text{Ni}_{0.40}\text{Cu}_{0.60}\text{Cr}_2\text{O}_4$ the AF1 transition occurs slightly above T_{FI} , where the ferrimagnetic coupled moments of the FI order are almost compensated. The spontaneous increase of magnetization of the AF phase is again shown in the enlarged $M(T)$ curve shown above. (c) A sharp increase in the $M(T)$ curve occurs for $\text{Ni}_{0.50}\text{Cu}_{0.50}\text{Cr}_2\text{O}_4$, where the AF1 and FI transitions set in practically at the same temperature (marked with a red vertical line). (d) In $\text{Ni}_{0.70}\text{Cu}_{0.30}\text{Cr}_2\text{O}_4$ the AF1 transition is observed well below T_{FI} . A slight spontaneous increase of M indicates the onset of the AF1 ordering.

Most remarkable is the antiferromagnetic Cr order on the orthorhombic distorted pyrochlore lattice for samples in the range between $x(\text{Cu}) = 0$ to 0.12. In Ref. [20] it was reported that the commensurate magnetic ordering in the Cr sublattice undergoes a change from a structure with $\mathbf{k}_{\text{AF2}} = (0,0,1)$ to another one with $\mathbf{k}_{\text{AF1}} = 0$, but no details about the transformation process were given. A further study on the end member NiCr_2O_4 and the mixed chromite $\text{Ni}_{0.98}\text{Cu}_{0.02}\text{Cr}_2\text{O}_4$ revealed that the magnetic ordering is even more complex due the coexistence of several magnetic phases and their complex temperature behavior [21]. This led us to determine the magnetic properties of several samples in the range from $x(\text{Cu}) = 0$ to 0.12 by magnetization measurements and neutron powder-diffraction experiments. All samples show similar anomalies in the magnetization curve as described above for $\text{Ni}_{0.70}\text{Cu}_{0.30}\text{Cr}_2\text{O}_4$, where a weak spontaneous increase of magnetization indicates an AF1 transition of the Cr moments [Fig. 4(a)].

To investigate in detail the T -dependent changes of magnetic ordering we have collected neutron powder patterns of the same samples in the range between 2 and 45 K. The

thermal variation of magnetic Bragg reflection of some selected mixed chromites is shown in Fig. 5. All observed magnetic reflections could be indexed, and different coexisting magnetic phases could be distinguished by their propagation vectors \mathbf{k} . For samples with $x(\text{Cu}) \geq 0.09$ the observed anomalies in the magnetization curves could be assigned to the onset of the commensurate phase AF1 with the wave vector $\mathbf{k}_{\text{AF1}} = 0$, while for samples with $x(\text{Cu}) < 0.09$ to the onset of the incommensurate phase IC1 with $\mathbf{k}_{\text{IC1}} = (0,0,k_z)$. In the magnetic phase diagram shown in Fig. 3, only the transition temperatures $T_{\text{CR-AF}}$ of these two magnetic phases are plotted versus $x(\text{Cu})$. In Fig. 4 the results of the magnetization measurements are compared with the changes of lattice parameters vs T obtained from x-ray- and neutron-diffraction data. It should be recalled that the orthorhombic splitting in Ni-rich mixed chromites occurs in the ab plane that is the tetragonal plane in the higher symmetric space group $I4_1/amd$. Interestingly, strong magnetoelastic effects also appear in the ab plane which are strongly pronounced for the onset of the commensurate AF1 ordering with $\mathbf{k} = 0$ and not for the incommensurate one with

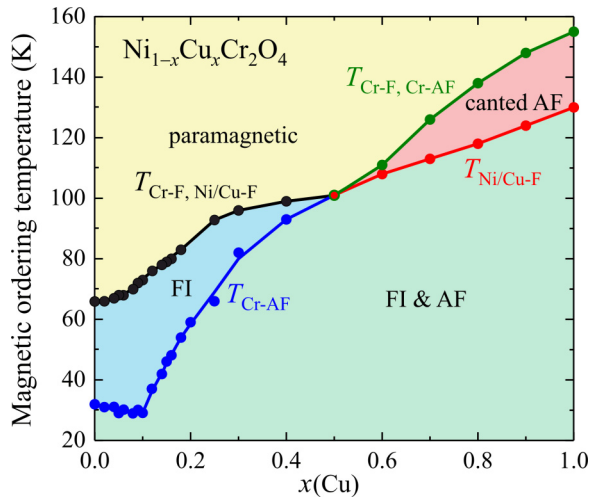


FIG. 3. Magnetic phase transitions from paramagnetism (yellow area) to long-range magnetic order obtained from $M(T)$ measurements and neutron powder-diffraction data. In the magnetic ground state, the ferrimagnetically (labeled as FI) coupled sublattices of the modes Cr-F and Ni/Cu-F coexist with the antiferromagnetic mode Cr-AF (green area). For Ni-rich samples with $x(\text{Cu}) < 0.5$ the FI transition sets in first followed by the AF transition at lower temperature (blue area). Conversely, for Cu richer samples with $x(\text{Cu}) > 0.5$ the ordering of Cr-F and Cr-AF modes sets in first forming a canted antiferromagnetic structure (red area). The ordering of the mode Ni/Cu-F sets in at lower temperature and couples ferrimagnetically with the mode Cr-F. For mixed chromites with $x(\text{Cu}) \leq 0.12$ the AF ordering of the Cr sublattice is rather complex as shown in Fig. 6. For a better overview only the transition temperatures T_{AF1} and T_{IC1} are plotted, where an anomaly is observed in the $M(T)$ curve. Interestingly, the strong decrease of T_{AF1} stops spontaneously at $x(\text{Cu}) = 0.10$, followed by a weak linear increase for T_{IC1} down to $x(\text{Cu}) = 0$.

$k_{\text{IC1}} = (0, 0, k_z)$. To make these effects visible the T dependence of the difference values $b - a$ are plotted in Fig. 4(b). An instability of the IC1 phase is observed in $\text{Ni}_{0.91}\text{Cu}_{0.09}\text{Cr}_2\text{O}_4$ which only exists in the T range between 19 and 28 K as shown in the antiferromagnetic phase diagram in Fig. 6, whereas it is well established down to 2 K in $\text{Ni}_{0.92}\text{Cu}_{0.08}\text{Cr}_2\text{O}_4$. The disappearance of phase IC1 in $\text{Ni}_{0.91}\text{Cu}_{0.09}\text{Cr}_2\text{O}_4$ finally stabilizes the commensurate phase AF1 with the wave vector $k_{\text{AF1}} = 0$, which is still absent in $\text{Ni}_{0.92}\text{Cu}_{0.08}\text{Cr}_2\text{O}_4$ (Fig. 6).

Further, the neutron diffraction data of several samples showed that the vector component k_z of phase IC1 does not change significantly with increasing temperature. On the other hand, the component k_z undergoes a continuous decrease in the concentration range from $x(\text{Cu}) = 0$ to 0.09, reaching finally an end value close to 0.5 as shown in Fig. 7(a). At this point one finds a sudden onset of the commensurate phase AF1 that is well established up to the end member CuCr_2O_4 . Interestingly, our neutron powder-diffraction experiments also revealed the existence of another incommensurate AF2 phase with the wave vector $k_{\text{IC2}} = (0, k_y, k_z)$ in the range from $x(\text{Cu}) = 0.06$ to 0.12. The values of the vector components were found to be around $k_y \sim 1/3$ and $k_z \sim 1/2$. In contrast to the incommensurate phase IC1 significant changes of the peak

positions can be observed in powder patterns shown in Fig. 5. More accurate values of k_y and k_z could be determined from our data analysis, where the T dependence of the two components is shown in Fig. 7. For the samples with $x(\text{Cu}) = 0.06, 0.08, \text{ and } 0.10$ the thermal variation of k_y and k_z is more or less pronounced. A further increased Cu content finally destabilizes this phase, where it only exists in $\text{Ni}_{0.88}\text{Cu}_{0.12}\text{Cr}_2\text{O}_4$ between 35 and 40 K. For $\text{Ni}_{0.91}\text{Cu}_{0.09}\text{Cr}_2\text{O}_4$ a spontaneous change of k_y and k_z sets in at about 22 K, which also affects the intensities of magnetic reflections. Here it is not clear whether this phase undergoes a phase separation or a spin reorientation.

Figure 6 shows that two coexisting commensurate magnetic phases AF2 and AF3 appear below the transition temperature T_{IC1} in a small $x(\text{Cu})$ range from 0 to 0.04. For the end member NiCr_2O_4 the incommensurate transition sets in at $T_{\text{IC1}} = 32$ K, followed by the transition into the phase with $k_{\text{AF2}} = (0, 0, 1)$ at $T_{\text{AF2}} = 29$ K and below into the phase $k_{\text{AF3}} = (1/2, 1/2, 1/2)$ at $T_{\text{AF3}} = 21$ K. A similar behavior was found for the mixed chromites $\text{Ni}_{0.98}\text{Cu}_{0.02}\text{Cr}_2\text{O}_4$ and $\text{Ni}_{0.96}\text{Cu}_{0.04}\text{Cr}_2\text{O}_4$, although the difference between T_{AF2} and T_{AF3} is considerably reduced. A second anomaly is observed in the magnetization curve of $\text{Ni}_{0.98}\text{Cu}_{0.02}\text{Cr}_2\text{O}_4$ in Fig. 4(a). This indicates the onset of the commensurate phase of type AF3 with $k_{\text{AF3}} = (1/2, 1/2, 1/2)$ at 21 K as reported earlier in Ref. [21]. Our neutron powder data revealed that this phase coexists with AF2 up to $x(\text{Cu}) = 0.04$, but it is only strongly established in $\text{Ni}_{0.98}\text{Cu}_{0.02}\text{Cr}_2\text{O}_4$. Therefore, no second anomaly in the magnetization curve is observable for NiCr_2O_4 and $\text{Ni}_{0.96}\text{Cu}_{0.04}\text{Cr}_2\text{O}_4$ [Fig. 4(a)]. If we follow the magnetic ordering in the magnetic ground state at 2 K in the $x(\text{Cu})$ range from 0 to 0.14, it can be seen in Fig. 6 that the commensurate phases AF2 and AF3 undergo a change into the commensurate AF1 with $k_{\text{AF1}} = 0$ via two incommensurate phases with $k_{\text{IC1}} = (0, 0, k_z)$ and $k_{\text{IC2}} = (0, k_y, k_z)$.

C. Magnetic moments

In the following, we discuss the ferrimagnetically coupled moments of the Ni/Cu and the Cr sublattices of several mixed chromite samples in the magnetic ground state at 2 K. Magnetization measurements were performed to determine the net spontaneous magnetization $M_0 = M(\text{Ni/Cu}) - 2M(\text{Cr})$. Complete hysteresis curves $M(H)$ were run with increasing and decreasing field strengths up to 14 T. The spontaneous magnetization M_0 was determined by the intersection of the tangent dM/dH at the largest field with the vertical $M(H = 0)$ axis as carried out earlier for the end member CuCr_2O_4 [22]. For each sample covering the entire $x(\text{Cu})$ range the obtained M_0 value was used as a constraint to determine the individual moments $\mu(\text{Ni/Cu})$ and $\mu(\text{Cr})$ from neutron powder data with higher accuracy, where this constraint helped to reduce strong correlations between the magnetic ordering parameters. This also affects the accuracy of the additional AF1 component in the Cr sublattice lying orthogonal to the antiparallel coupled moments $\mu(\text{Ni/Cu})$ and $\mu(\text{Cr})$ since both magnetic structures have the same wave vector $k = 0$.

Our neutron-diffraction study showed that the AF1 moments of Cr solely generate magnetic intensity at the position on the reflection 200. Therefore, the AF1 moment can be

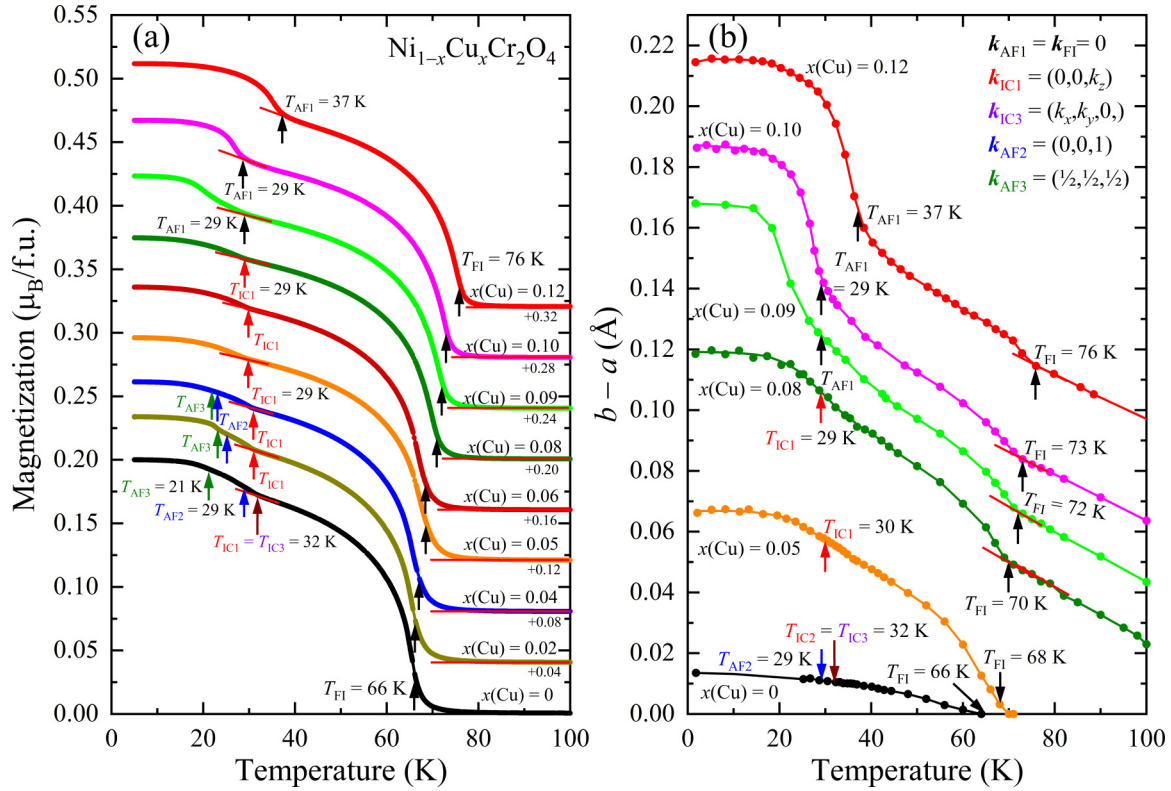


FIG. 4. Magnetization and orthorhombic distortion vs T for Ni-rich samples of $\text{Ni}_{1-x}\text{Cu}_x\text{Cr}_2\text{O}_4$ in the range from $x(\text{Cu}) = 0$ to 0.12. Arrows mark the positions of magnetic phase transitions determined from neutron powder-diffraction data (a) The magnetization was measured in a weak applied magnetic field of 0.05 T. A spontaneous increase of magnetization indicates the onset of FI ordering between 66 and 76 K. At lower temperatures an anomaly in the $M(T)$ curvature indicates the onset of AF ordering of the Cr^{3+} ions which is incommensurate up to $x(\text{Cu}) = 0.09$ and changes then to the commensurate phase with $k_{AF1} = 0$. Only for $\text{Ni}_{0.98}\text{Cu}_{0.02}\text{Cr}_2\text{O}_4$ another anomaly appears at the transition into the phase with $k_{AF2} = (\frac{1}{2}, \frac{1}{2}, \frac{1}{2})$, where this magnetic phase is most pronounced. (b) The orthorhombic distortion is evidenced by the splitting by the lattice parameters a and b , shown as $b - a$. The FI transition in NiCr_2O_4 sets in concomitantly with the structural phase transition to the orthorhombic phase. For samples with $x(\text{Cu}) > 0.06$ a spontaneous increase of $b - a$ is observed, while the structural phase transition strongly shifts to higher temperature. A further sharp increase is only observed for the onset of commensurate ordering with $k_{AF1} = 0$.

directly derived from the integrated magnetic intensity of this reflection. This could be used as a further constraint to determine the antiparallel coupled moments $\mu_{FI}(\text{Ni}/\text{Cu})$ and $\mu_{FI}(\text{Cr})$ in the magnetic ground state at 2 K with even better accuracy. In Fig. 8(b) these moments are plotted versus $x(\text{Cu})$ together with the moments $\mu_{AF1}(\text{Cr})$. Due to the used constraints and the larger number of measured samples, this diagram now provides a more detailed representation of the $x(\text{Cu})$ -dependent changes of the individual moments than in our earlier work [20]. Now it can be clearly seen that the magnetic moment of the A^{2+} -site ion shows at 2 K a linear increase from 0.83(4) to 2.28(2) μ_B in the range from $x(\text{Cu}) = 1$ down to 0.15, where the orthorhombic distortions are most pronounced. The moment of Cu^{2+} is somewhat smaller than the theoretical spin-only value $\mu_S = 1 \mu_B$. Assuming for $\text{Ni}_{0.85}\text{Cu}_{0.15}\text{Cr}_2\text{O}_4$ the same moment of the Cu^{2+} ion as determined for CuCr_2O_4 , one obtains for Ni^{2+} a moment of 2.5(1) μ_B , which is somewhat larger than the theoretical spin-only value $\mu_S = 2 \mu_B$, where the enlarged moment may be caused by an additional contribution from the orbital momentum. Conversely, a further increasing Ni content up to the end member NiCr_2O_4 leads to a continuous decrease of the A^{2+} site moment, where finally the Ni^{2+} ion reaches a smaller

moment of 2.08(3) μ_B . This value is in good agreement with the value 2.0 μ_B obtained earlier in Ref. [27]. Figure 8(b) shows that a similar decrease is observed for the antiparallel coupled Cr moment, indicating that the two FI moments are strongly coupled. But interestingly, the decrease of the AF1 component of Cr is much stronger pronounced in the range from $x(\text{Cu}) = 0.15$ to 0.09. This indicates that decreasing lattice distortions cause geometrical frustration in the corner-shared network of Cr^{3+} ions and consequently a reduction of the Cr moments. On the other hand, the changes of the FI and AF moments of Cr are only weakly defined in the large range from $x(\text{Cu}) = 0.15$ to 1. Here it can be seen that geometrical frustration is prevented by strongly acting Jahn-Teller effects on the Ni^{2+} and Cu^{2+} ions at the A site due to strongly pronounced orthorhombic and tetragonal distortions.

In agreement with the results of Ref. [20], it is shown that the moment direction of the FI ordering was parallel to the a axis up to $x(\text{Cu}) = 0.90$. Only for the end member CuCr_2O_4 an unusually enlarged ferrimagnetically coupled Cr moment was determined from neutron powder data, resulting in a much larger M_0 value compared to that obtained earlier from magnetization measurements [10]. In Ref. [22] a

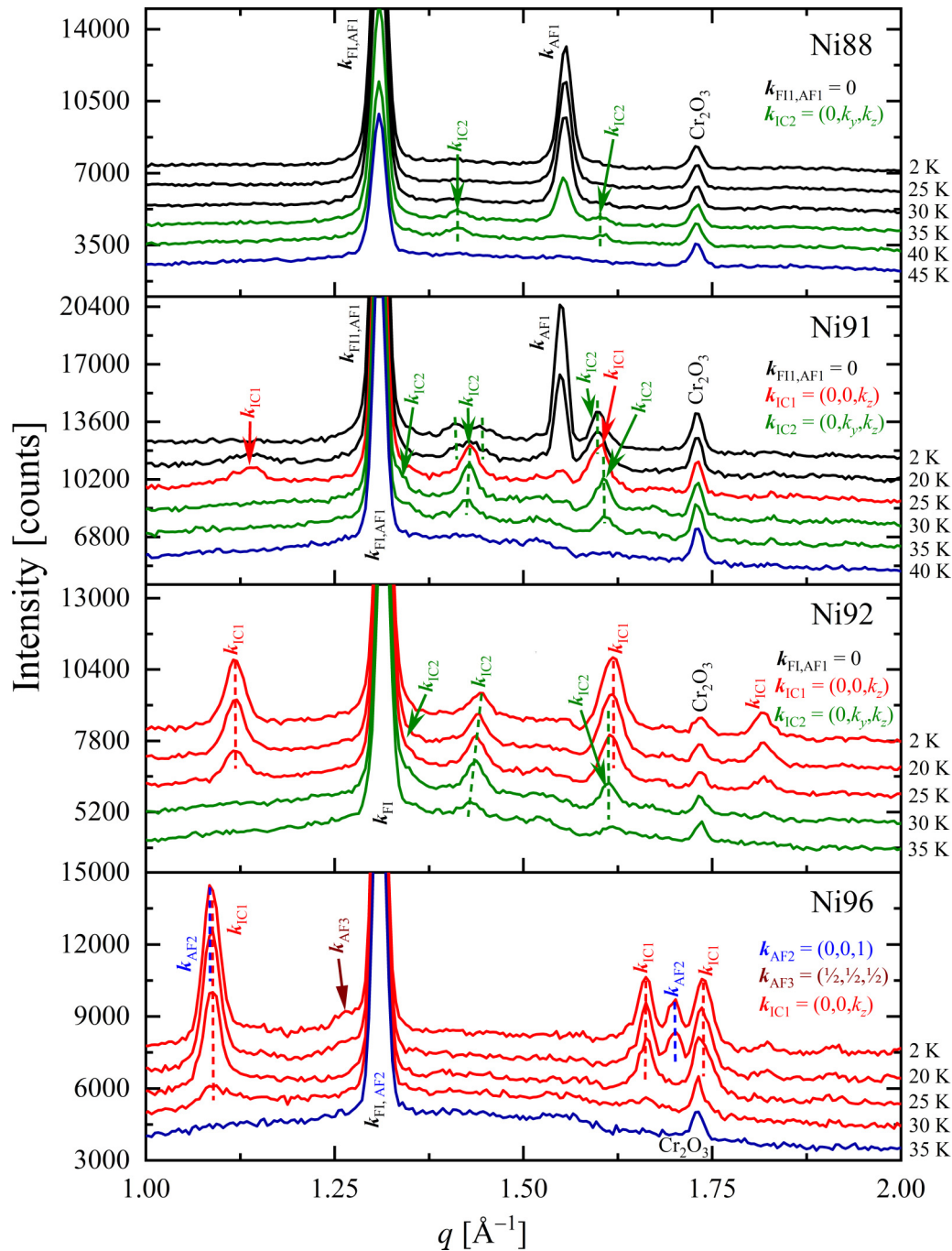


FIG. 5. Neutron powder patterns Ni-rich chromites collected on E2 showing the complex thermal variation of commensurate and incommensurate AF ordering. With increasing Cu content the AF ordering undergoes a change of the commensurate spin structures, where the vectors $k_{\text{AF2}} = (0, 0, 1)$ and $k_{\text{AF3}} = (\frac{1}{2}, \frac{1}{2}, \frac{1}{2})$ change to $k_{\text{AF1}} = 0$. This transition is accompanied by the occurrence of incommensurate magnetic phases with the vectors $k_{\text{IC1}} = (0, 0, k_z)$ and $k_{\text{IC2}} = (0, k_y, k_z)$.

satisfactory agreement between the two methods can be obtained for CuCr_2O_4 , where the direction of the ferrimagnetically coupled moments is changed from the a to the b axis. In the present study it is shown that this spin reorientation occurs above $x(\text{Cu}) \approx 0.95$ [Fig. 8(b)]. Here, it can be seen that the ferrimagnetically coupled moments $\mu(\text{Ni}/\text{Cu})$ and $\mu(\text{Cr})$ continuously decrease with increasing Cu content up to the end member CuCr_2O_4 .

As already mentioned above, the AF ordering in the Cr sublattice is rather complex in the range from $x(\text{Cu}) = 0$ to 0.12

due to the occurrence of coexisting magnetic phases. For the end member NiCr_2O_4 a reduced total moment $1.49(4) \mu_B$ was obtained for Cr, where for the calculation only the magnetic moment of the AF2 phase with $k = (0, 0, 1)$ was considered in Ref. [20]. A much larger moment of $2.7(1) \mu_B$ is reported in Ref. [21], where additionally the two coexisting phases with $k_{\text{IC1}} = (0, 0, k_z)$ and $k_{\text{AF3}} = (\frac{1}{2}, \frac{1}{2}, \frac{1}{2})$ were taken into account. As described above very reliable values of the total moment of the Cr^{3+} ions could be determined in the range between $x(\text{Cu}) = 0.10$ and 1. It is interesting to see, that the

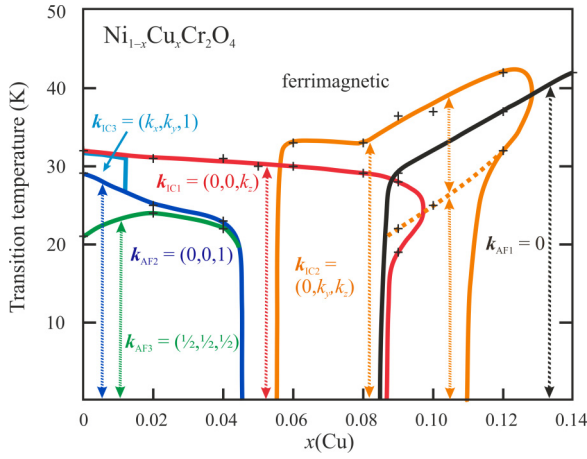


FIG. 6. Antiferromagnetic phase diagram of $\text{Ni}_{1-x}\text{Cu}_x\text{Cr}_2\text{O}_4$ from $x(\text{Cu}) = 0$ to 0.14. All magnetic phases are denoted by their wave vectors. In this range incommensurate (IC) magnetic phases appear first with decreasing temperature. In the case of NiCr_2O_4 two incommensurate phases IC1 and IC3 are observed [21], followed by a change to the commensurate phases AF2 and AF3. A substitution of Ni by Cu leads to a transition via the incommensurate phases IC1 and IC2, and it finally changes to the commensurate one, AF1. In the range from $x(\text{Cu}) = 0.06$ to 0.12 another incommensurate phase IC2 is observed coexisting with the phases IC1 and AF1. In the range from $x(\text{Cu}) = 0.08$ to 0.12 phase IC2 undergoes a second magnetic transition (marked with the dashed orange line) possibly due to a spin reorientation.

moments remain practically unchanged and only vary in this range between 2.38(2) and 2.45(2) μ_B . It can be assumed that the maximum moment is reached in this range, where the orthorhombic and tetragonal distortions are most pronounced. Therefore, the moment of 2.7(1) μ_B obtained for NiCr_2O_4 seems to be too large since the lattice distortions are less pronounced. This already indicates that the determination of the total Cr moment is delicate in the range from $x(\text{Cu}) = 0$ to 0.12. Nevertheless, it can be concluded that all obtained total Cr moments are considerably smaller than the theoretical spin-only moment $\mu_S = 3.0 \mu_B$ of the Cr^{3+} ion. Further, it has to be mentioned that our data analysis did not allow a reliable determination of the Cr moments for some coexisting phases, especially for incommensurate ones. This can be ascribed to the fact that intensities of the magnetic reflections are relatively weak and the fact that in some cases magnetic reflections could not be clearly separated due to strong peak overlaps. However, in the case of $\text{Ni}_{0.95}\text{Cu}_{0.05}\text{Cr}_2\text{O}_4$ only the incommensurate magnetic phase IC1 with $\mathbf{k}_{\text{IC1}} = (0, 0, k_z)$ coexists with the FI phase, which exhibits a sine-wave modulated ordering. For the phase IC1 and FI we obtained the Fourier components $\mu_z = 1.61(4) \mu_B$ and $\mu_x = 0.92(1) \mu_B$ resulting in a total moment of the Cr^{3+} ions $\mu_{\text{tot}} = 1.85(5) \mu_B$ that is again considerably smaller than the theoretical spin-only moment $\mu_S = 3.0 \mu_B$ of the Cr^{3+} ion. In the case of the FI phase the Fourier component is identical to the ordered moment, while the ordered moment of IC1 may be even smaller due to its incommensurability. For the samples containing the other incommensurate IC2 phase with the wave vector $\mathbf{k}_{\text{IC2}} = (0, k_y, k_z)$ it has to be mentioned that

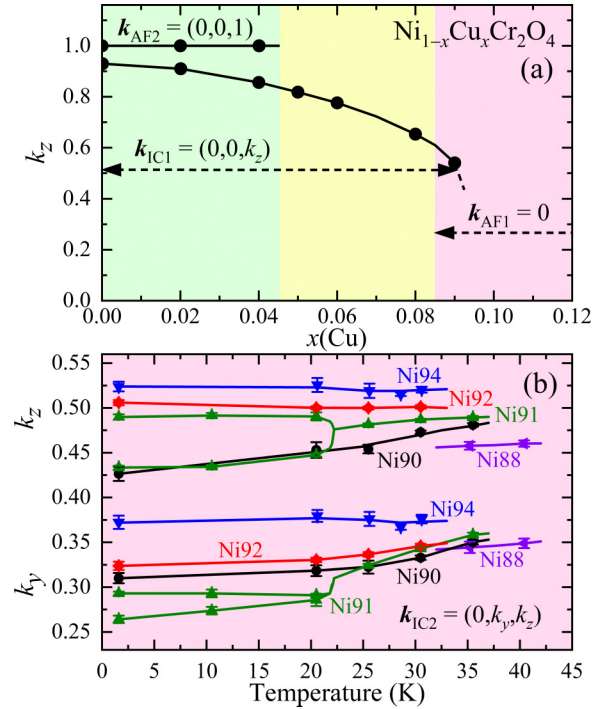


FIG. 7. (a) Change of the k_z component of the propagation vector $\mathbf{k}_{\text{IC1}} = (0, 0, k_z)$ with increasing Cu content from $x(\text{Cu}) = 0$ to 0.12. Up to $x(\text{Cu}) \sim 0.04$ this phase coexists with the antiferromagnetic phase AF2. It is found that the magnetic phase IC1 at $x(\text{Cu}) = 0.09$ only occurs in the temperature range between 19 and 28 K which is coexisting with the phase AF1. The k_z components of each sample do not show significant changes vs T . (b) Thermal variation of the k_y and k_z components of the propagation vector $\mathbf{k}_{\text{IC2}} = (0, k_y, k_z)$ in the range from $x(\text{Cu}) = 0.06$ to 0.12.

the magnetic structure could not be fully determined, with the consequence that the total Cr moment is yet unknown. Due to all these difficulties, only the AF1 moments are plotted versus $x(\text{Cu})$ in Fig. 8 together with the two ferrimagnetically coupled moments $\mu(\text{Ni}/\text{Cu})$ and $\mu(\text{Cr})$.

D. AF ordering in the Cr sublattice

Before continuing with the analysis of magnetic structures, we recall the symmetry of the crystal structure of the mixed chromite samples in the magnetic ground state. In the entire concentration range of the system $\text{Ni}_{1-x}\text{Cu}_x\text{Cr}_2\text{O}_4$ all samples have an orthorhombic structure with the space group $Fmmm$. For CuCr_2O_4 the orthorhombic splitting in the bc plane is rather weak and it was only proved in an earlier high-resolution synchrotron diffraction study [10]. In the present work we use the setting of the cell with the dimensions $a < b \leq c$, where a is the tetragonal axis in the next-higher symmetry. This is the notation of the tetragonal setting of NiCr_2O_4 , where c is the tetragonal axis as standard. Due to the rather weak splitting of the lattice parameters b and c in the range down to $x(\text{Cu}) = 0.50$, the crystal structure was refined in the tetragonal space group $I4_1/amd$. This pseudotetragonal structure with an almost linear $x(\text{Cu})$ dependence of the lattice constant c exists between $x(\text{Cu}) = 0.40$ and 1, where the orthorhombic splitting becomes evident for samples

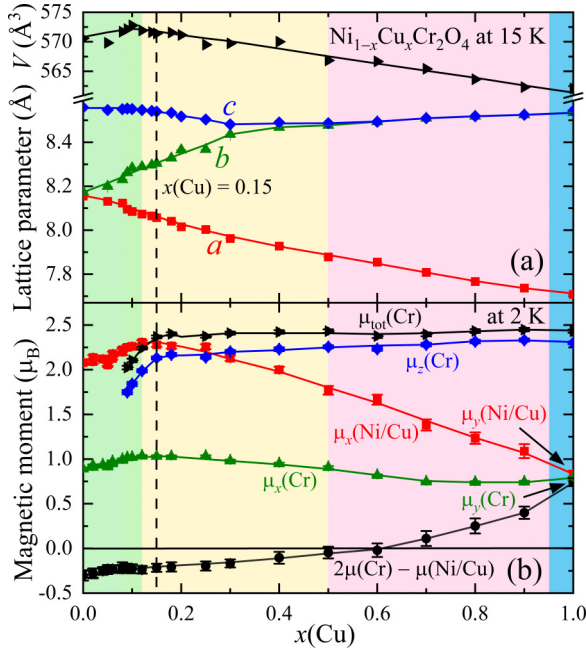


FIG. 8. (a) The influence of increasing Cu content on the change of lattice parameters in the mixed system $\text{Ni}_{1-x}\text{Cu}_x\text{Cr}_2\text{O}_4$. For $\text{Ni}_{0.85}\text{Cu}_{0.15}\text{Cr}_2\text{O}_4$ one finds the strongest orthorhombic distortions (marked with a vertical dashed line). (b) Change of the ferrimagnetically coupled moments $\mu(\text{Cr})$ and $\mu(\text{Ni/Cu})$ and the resulting ferromagnetic moments $2\mu(\text{Cr}) - \mu(\text{Ni/Cu})$ as a function of $x(\text{Cu})$. A compensation of both components is reached at $x(\text{Cu}) = 0.60$. A spin reorientation sets in above $x(\text{Cu}) = 0.95$, where the moment direction of the FI component changes from the a to the b axis (blue area) [12]. In the Ni-rich mixed chromites a complex antiferromagnetic ordering is observed for the Cr^{3+} ions from $x(\text{Cu}) = 0$ to 0.12 (green area) which is described in more detail in Fig. 6. In the green and yellow areas the AF ordering of the Cr moments sets in below the ordering temperature T_{FI} , whereas in the red and blue areas F and AF ordering of the Cr moments sets in above T_{FI} .

with $x(\text{Cu}) \leq 0.40$ as shown in Fig. 8(a). In the region $x(\text{Cu}) \leq 0.40$ the two long lattice axes b and c show a strongly increasing orthorhombic splitting, where b converges almost linearly towards the short a axis [Fig. 8(a)]. For the other end member NiCr_2O_4 also weak orthorhombic distortions remain in the unit cell with the dimensions $a \leq b < c$ [10]. The largest orthorhombic distortion occurs around $x(\text{Cu}) = 0.15$ as marked with a dashed line in Fig. 8(a), where the differences between all three lattice constants are comparable. The magnetically ordered Cr^{3+} ions are located at the Wyckoff position 16d [Cr1(1/2, 1/2, 1/2); Cr2(1/4, 1/4, 1/2); Cr3(1/4, 1/2, 1/4); and Cr4(1/2, 1/4, 1/4)] of the space group $Fddd$ (No. 70, cell choice 2). To simplify the calculation of the magnetic structure factor $F(hkl)$ of a Cr_4 tetrahedron, we used in Ref. [21] the following setting: Cr1(0,0,0); Cr2(1/4, 1/4, 0); Cr3(1/4, 0, 1/4); and Cr4(0, 1/4, 1/4).

In our earlier neutron diffraction study a comprehensive description of the structural and magnetic properties was reported for the entire concentration range of the mixed system $\text{Ni}_{1-x}\text{Cu}_x\text{Cr}_2\text{O}_4$ [20]. Two further studies gave a more detailed description of the magnetic structure of the end members NiCr_2O_4 and CuCr_2O_4 , where also the mag-

netic structure of the mixed chromites $\text{Ni}_{0.98}\text{Cu}_{0.02}\text{Cr}_2\text{O}_4$ and $\text{Ni}_{0.10}\text{Cu}_{0.90}\text{CuCr}_2\text{O}_4$ were investigated [21,22]. Here, the coexisting AF1 and FI phase order with the same propagation vector $\mathbf{k} = 0$ was described. Additionally, in the present study it is found that this type of ordering first occurs in $\text{Ni}_{0.91}\text{Cu}_{0.09}\text{Cr}_2\text{O}_4$ and remains stable up to the end member CuCr_2O_4 . In this large range the Cr moments of the AF1 phase are aligned parallel to the c axis, forming a spin sequence $+-+$, where c is always the largest axis in the entire range of the mixed system $\text{Ni}_{1-x}\text{Cu}_x\text{Cr}_2\text{O}_4$.

Now we focus our attention on the complex antiferromagnetic ordering in the pyrochlore lattice formed by Cr atoms in the $x(\text{Cu})$ range from 0 to 0.12. In Refs. [20] and [27] the magnetic structure of NiCr_2O_4 was described with the propagation vector $\mathbf{k} = (0,0,1)$ labeled as AF2 in the present work. As found above for the AF1 phase with $\mathbf{k} = 0$ the Cr moments are again aligned parallel to the c axis and with the same spin sequence $+-+$. In a further study it was reported that two other magnetic phases coexist in NiCr_2O_4 with AF2: A commensurate phase with $\mathbf{k}_{\text{AF3}} = (\frac{1}{2}, \frac{1}{2}, \frac{1}{2})$ and an incommensurate one with $\mathbf{k}_{\text{IC1}} = (0,0,k_z)$, where k_z reaches in NiCr_2O_4 a value of 0.93(1) [21]. In the present study it is shown that phase AF3 only exists up to the low Cu content of $x(\text{Cu}) = 0.04$, where it is most pronounced in $\text{Ni}_{0.98}\text{Cu}_{0.02}\text{Cr}_2\text{O}_4$. The data analysis reveals that the Cr lattice is divided into two sublattices according to the different chain directions in the ab plane, where the spin pairs $S_{\text{Cr1}}-S_{\text{Cr2}}$ belong to sublattice I ($SL-I$), and $S_{\text{Cr3}}-S_{\text{Cr4}}$ to $SL-II$, respectively. In each sublattice one finds an antiparallel spin arrangement $(+ -)$. The magnetic structures of $SL-I$ are described with the propagation vectors $\mathbf{k} = (0,0,1)$ and $\mathbf{k}_{\text{IC1}} = (0,0,k_z)$, while $SL-II$ is described with $\mathbf{k}_{\text{AF3}} = (\frac{1}{2}, \frac{1}{2}, \frac{1}{2})$ [11].

In our present study it is shown that first deviations from the AF1 structure $\mathbf{k}_{\text{AF1}} = 0$ appear in $\text{Ni}_{0.88}\text{Cu}_{0.12}\text{Cr}_2\text{O}_4$ in the form of a modulated spin structure with a wave vector $\mathbf{k}_{\text{IC2}} = (0, k_y, k_z)$ followed by another modulated one with $\mathbf{k}_{\text{IC2}} = (0,0,k_z)$ below $x(\text{Cu}) = 0.10$. For both it can be shown that satellite reflections appear around the reflection 200 labeled as $(200)^\pm$, while they are extinct around 020 and 002. This is closely related to the observation for the AF1 phase with $\mathbf{k} = 0$, where magnetic intensity appears straight on the 200, but not on the 020 and 002. It is important to note that the spin order of a single tetrahedron is entirely determined by the spins of the surrounding four corner-connected Cr_4 tetrahedra, each sharing a common Cr^{3+} ion. This structural property divides the Cr_4 tetrahedra into two groups, labeled as **A** and **B**. Thus, the spin arrangement on the **A** tetrahedra and the wave vector completely determine the magnetic structure of the entire crystal lattice. The extinction rules $F(020) = 0$ and $F(002) = 0$ for the phase $\mathbf{k} = 0$ are, respectively, preserved for the IC satellites if the spin ordering on a single **A** tetrahedron remains the same. This is achieved by spatially independent phase shifts between the four Cr^{3+} ions, which compensate for the spatially dependent phase shifts produced by the IC components of the scattering vector. The magnetic structure factor defined as $F(\mathbf{k}) = \sum S_j \exp(-2\pi i \mathbf{k} \cdot \mathbf{r}_j)$ is calculated for $\mathbf{k} = 0$ as follows: $2S_1 - 2S_3$ for $F(200)$, $2S_1 + 2S_3$ for $F(020)$, and zero for $F(002)$. The lattice vectors \mathbf{r}_j of the Cr^{3+} ions are defined on a single tetrahedron as given above. For $\text{Ni}_{0.88}\text{Cu}_{0.12}\text{CuCr}_2\text{O}_4$ we assume $\mathbf{S}_2 = -\mathbf{S}_1$ and $\mathbf{S}_4 = -\mathbf{S}_3$ for

spin pairs lying on the diagonals in the tetragonal ab plane. The net moment in the plane is zero and $F(002) = 0$. If $\mathbf{S}_3 = -\mathbf{S}_1$, $F(020) = 2\mathbf{S}_1 + 2\mathbf{S}_3$ vanishes, and $F(200) = 4\mathbf{S}_1$ is different from zero. The extinction of the 020 reflection for the AF phase with $\mathbf{k} = 0$ requires that all Cr^{3+} ions on the four sites must have magnetic moments of equal size. ‘‘Phase compensation’’ preserves the zero net moment on the **A** tetrahedra. Different is the spin order on the **B** tetrahedra, which vary in their spin sizes. Reductions in the ordered moment generate entropy [28]. This is one reason why IC structures can be favored at high temperatures and convert to commensurate structures as the temperature decreases. The wave vector $\mathbf{k} = (0, k_y, k_z)$ with $k_y \sim 1/3$ and $k_z \sim 1/2$ generates only spin modulation along b and c . The modulation along b is less than along c . For a sinusoidal spin modulation, the exchange energy decreases with increasing difference in the spin size of neighboring Cr^{3+} ions. The spin-size modulations only occur between different **A** tetrahedra and are transmitted within the **B** tetrahedra. In addition, the AF coupling constant $J(r)$ depends on the Cr-Cr distance r and influences the energy of the AF structure. A decrease in r will probably strengthen AF bonds for $\text{Ni}_{1-x}\text{Cu}_x\text{Cr}_2\text{O}_4$ [4].

E. Magnetoelastic effect

Next, we look to lattice strains induced by magnetic order. The magnetoelastic behavior is examined on selected samples with $x(\text{Cu}) = 0.60, 0.75$, and 0.82 using data collected on KMC-2. $\text{Ni}_{0.60}\text{Cu}_{0.40}\text{Cr}_2\text{O}_4$ has a weakly distorted orthorhombic lattice which is treated in this study as a tetragonal one. In contrast, the orthorhombic distortions in $\text{Ni}_{0.75}\text{Cu}_{0.25}\text{Cr}_2\text{O}_4$ and $\text{Ni}_{0.82}\text{Cu}_{0.18}\text{Cr}_2\text{O}_4$ are well established. We follow the conventional symmetry-breaking strains given by Kataoka and Kanamori [29]:

$$\begin{aligned} e_{\text{tetra}} &= (1/\sqrt{6})(2e_{33} - e_{11} - e_{22}) \text{ and } e_{\text{ortho}} \\ &= (1/2)^{1/2}(e_{11} - e_{22}), \end{aligned}$$

where e_{ii} are the associated diagonal elements of the elastic strain tensor along the crystallographic axes a , b , and c , where $e_{11} = (a - a_0)/a_0$, $e_{22} = (b - a_0)/b_0$, and $e_{33} = (c - a_0)/a_0$. The reference cubic cell parameter a_0 is determined by fitting the curve progression above the phase transition and then extrapolating to lower temperature in the tetragonal or orthorhombic phase. The presence of magnetoelastic strain is investigated for the FI-, canted AF-, and AF-phase transitions. The magnetoelastic strains are determined from the T -dependent lattice distortions above and below the ordering temperature. Above the ordering temperature the data are fitted to a second-order polynomial. In many cases the quadratic part is found to be much lower than the linear term. The fit function is extrapolated to lower temperatures and the difference to the measured distortions with the onset of the spin order determines the magnetoelastic strain. To compare transitions at different temperatures, the data are plotted as a function of the reduced temperatures $T_{\text{red}} = (T - T_{\text{tetra}})/T_{\text{tetra}}$ and $T_{\text{red}} = (T - T_{\text{ortho}})/T_{\text{ortho}}$ for the tetragonal and the orthorhombic case, respectively. $\text{Ni}_{0.60}\text{Cu}_{0.40}\text{Cr}_2\text{O}_4$ remains in an almost tetragonal structure during the magnetic transitions. For this chromite our data do not allow to distinguish between strains produced by antiferromagnetism and ferrimagnetism

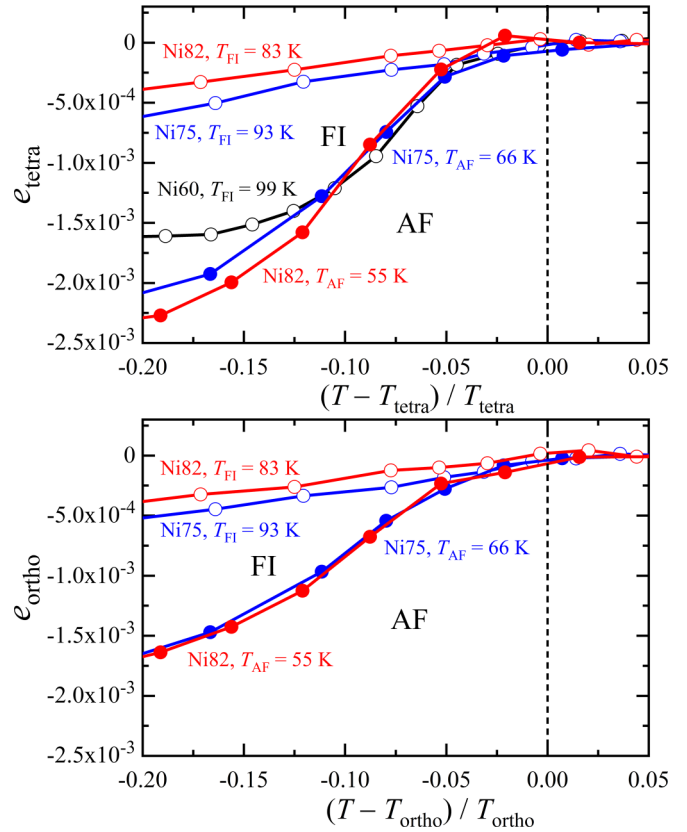


FIG. 9. Tetragonal and orthorhombic strain in $\text{Ni}_{0.60}\text{Cu}_{0.40}\text{Cr}_2\text{O}_4$, $\text{Ni}_{0.75}\text{Cu}_{0.25}\text{Cr}_2\text{O}_4$, and $\text{Ni}_{0.82}\text{Cu}_{0.18}\text{Cr}_2\text{O}_4$ as a function of reduced ordering temperature. The e_{ortho} and e_{tetra} strains show a linear dependence on reduced temperatures $(T - T_{\text{tetra}})/T_{\text{tetra}}$ and $(T - T_{\text{ortho}})/T_{\text{ortho}}$ for ferrimagnetism, while both strains show a quadratic dependence at the AF transition. Open circles refer to the FI transition; full circles refer to AF transition. Symbol sizes correspond to the error bars.

because both transitions $T_{\text{AF}} = 93$ K and $T_{\text{FI}} = 99$ K are close together. The observed magnetoelastic strain adapts the tetragonal symmetry and has a value of about 0.001 for $T_{\text{red}} = 0.1$ (Fig. 9). For $\text{Ni}_{0.75}\text{Cu}_{0.25}\text{Cr}_2\text{O}_4$ and $\text{Ni}_{0.82}\text{Cu}_{0.18}\text{Cr}_2\text{O}_4$ the crystal structure is clearly orthorhombic. Here, ferrimagnetism occurs at 93 and 83 K, well above the AF transitions 66 and 55 K. The e_{ortho} and e_{tetra} strains show a linear dependence on T_{red} for ferrimagnetism, while both strains show a quadratic dependence at the AF transition. In both cases, the strains caused by antiferromagnetism are more pronounced. The concentration dependence of strain between the samples $\text{Ni}_{0.75}\text{Cu}_{0.25}\text{Cr}_2\text{O}_4$ and $\text{Ni}_{0.82}\text{Cu}_{0.08}\text{Cr}_2\text{O}_4$ is small. If one considers the temperature-dependent magnetic intensity of the reflection $(111)_{\text{M}}$ due to ferrimagnetic, one recognizes an approximately linear T dependence shown in Fig. 6 of Ref. [20], which is also found for the magnetoelastic strain. Since the Bragg intensity $\text{Int}(111)_{\text{M}} \sim M^2$, it is interesting to see that also the strain becomes $e \sim M^2$, which is discussed below in Sec. IV. The same is concluded for antiferromagnetism, where $\text{Int}(200)_{\text{M}}$ and the associated magnetoelastic strain both show a squared T dependence.

IV. DISCUSSION AND CONCLUSION

The structural and magnetic properties of NiCr_2O_4 and CuCr_2O_4 significantly differ due to their opposing Jahn-Teller distortions in the Ni^{2+} and Cu^{2+} tetrahedra, although the Cr moments are always oriented parallel to the largest crystallographic axis of unit cell as observed in typical Ising-type antiferromagnets. In the lattice of NiCr_2O_4 the strongest AF bonds with the shortest distance between the Cr^{3+} ions form two diagonal chains along the directions $[110]$ and $[1\bar{1}0]$ lying perpendicular to the elongated tetragonal axis (Fig. 1). A coupling between these two chains can occur in different ways via the remaining four bonds in the Cr_4 tetrahedron (ground-state degeneracy). The collinearity of spins only allows F and AF bonds. A shortened tetragonal axis of CuCr_2O_4 leads to a compressed Cr_4 tetrahedron with four equally strong AF bonds, where now the two weaker magnetic bonds within the tetragonal plane become F coupled. There is no macroscopic degeneration of magnetic states. Measurements of the lattice constants at low temperatures [10] together with the formation of the canted Cr-AF order [22] show that the magnetoelastic strain enhances the JT-induced tetragonal distortion. The AF mode, with four strong AF bonds on the side faces of the Cr_4 tetrahedron, increases lattice compression while maintaining fourfold local symmetry. Something similar is to be expected for the six F bonds of the Cr-F mode, since the JT distortion also splits the couplings into a quartet and a doublet. However, at 130 K a continuous transition to an orthorhombic lattice is observed. At this temperature the Cu-F mode occurs. The T dependence of the lattice constant b shows a kink and becomes almost independent of temperature below 130 K, while a and c do not change their T dependence in a linear approximation [10]. Therefore, in addition to the observed “orthorhombic” lattice splitting at the ferrimagnetic transition, there is a tetragonal strain that counteracts the tetragonal JT distortion. The reduction in tetragonal distortion and the associated increase in orthorhombicity indicate a change in the proportion between the two strain components. Also remarkable is the sudden increase in Cr-AF moment at the Cu-F transition shown in Fig. 2 of Ref. [22] that suggests coupling between Cr-F and Cr-AF. This contribution to Cr-AF further increases the JT distortion. Possible superexchange pathways for the Cu-F mode to account for Cu-F order will involve two bridging oxygen atoms along the edge of the oxygen octahedron or O-Cr-O transfer via the central Cr ion in the oxygen octahedron (Fig. 1). These are expected to be small. We mention that Cu-F always occurs together with a Cr-F mode. Therefore, the Cu-O-Cr superexchange is likely to be the dominant coupling that produces ferrimagnetism and is thus responsible for the long-range Cu magnetic ordering. Next, we turn to the magnetoelasticity of NiCr_2O_4 . Ferrimagnetism occurs around 60 K accompanied by an orthorhombic lattice distortion [10]. Below the FI transition, the two small identical lattice constants split into an upper $b(T)$ and a lower $a(T)$ branch. The upper branch experiences only a small increase in its temperature dependence at the transition, while the decrease in the lower branch is larger. This tetragonal strain amplifies the tetragonal JT distortion.

We now discuss our current results on the mixed system $\text{Ni}_{1-x}\text{Cu}_x\text{Cr}_2\text{O}_4$. Due to the limited instrumental resolution,

we only have access to magnetoelastic orthorhombic strains for samples with a JT-induced orthorhombic distortion that sufficiently separates the lattice constants a , b , and c at the magnetic transitions. This is the case for samples with higher Ni content than $\text{Ni}_{0.70}\text{Cu}_{0.30}\text{Cr}_2\text{O}_4$. In Fig. 9 we show the orthogonal and tetragonal strains for $\text{Ni}_{0.75}\text{Cu}_{0.25}\text{Cr}_2\text{O}_4$ and $\text{Ni}_{0.82}\text{Cu}_{0.18}\text{Cr}_2\text{O}_4$, and for comparison the tetragonal strain of $\text{Ni}_{0.60}\text{Cu}_{0.40}\text{Cr}_2\text{O}_4$. As mentioned above, all strain parameter e follows the relationship $e \sim M^2$. This behavior results from the competition between an elastic recovery energy that depends quadratically and an exchange energy $J(r)S_iS_j$ that depends linearly on the strain. Minimizing the total energy gives the equilibrium strain [12]. The strains e_{tetra} for the three mixed chromites at the lower AF transition amplify the structurally present tetragonal JT distortion. The same is valid at the FI transition for $\text{Ni}_{0.75}\text{Cu}_{0.25}\text{Cr}_2\text{O}_4$ and $\text{Ni}_{0.82}\text{Cu}_{0.18}\text{Cr}_2\text{O}_4$ as well as for all distortions (strains) of orthorhombic symmetry.

Before considering the rather complex behavior of the AF order with a variety of different magnetic phases on the Ni-rich side, we begin with a discussion of antiferromagnetic Cr order for Ni-richer chromites than $\text{Ni}_{0.96}\text{Cu}_{0.04}\text{Cr}_2\text{O}_4$. The AF structure on the single tetrahedron contains four AF and two F bonds. On the other hand, chromites with lower Ni content than $\text{Ni}_{0.70}\text{Cu}_{0.30}\text{Cr}_2\text{O}_4$ are tetragonal (neglecting the orthorhombic distortion due to ferrimagnetism) and the four AF bonds form a low-energy quartet and a high-energy F doublet. The compressed JT tetrahedra for Cu and the stretched ones for Ni minimize the elastic energy in the mixed crystals by an arrangement in which the long axis for Ni favors an alignment to one of the two long axes for Cu [29,30]. Due to the stronger JT distortion for Cu, the retention of the tetragonal structure down to $\text{Ni}_{0.60}\text{Cu}_{0.40}\text{Cr}_2\text{O}_4$ becomes plausible. For chromites with lower Ni content than $\text{Ni}_{0.60}\text{Cu}_{0.40}\text{Cr}_2\text{O}_4$ the crystal structure is orthorhombic. Now the energy of the four AF bonds splits into two doublets of different energies. The magnetic structure remains with increasing Ni content up to $\text{Ni}_{0.91}\text{Cu}_{0.09}\text{Cr}_2\text{O}_4$ in the AF phase with $k = 0$. This indicates that a rather large stretching of the tetrahedron with correspondingly large energy differences in magnetic binding energies are required to select one plane, the ab plane, solely with AF bonds, compared to prioritizing AF couplings on two faces and forcing F coupling only to the bc plane in the case of a compressed tetrahedron.

The tetragonal part of the JT distortion increases with increasing Ni content, while the orthorhombic part decreases. We now look to a correlation between JT distortions and the development of antiferromagnetism. With respect to that, the magnetic bond strengths for IC phase reflect orthorhombicity in their symmetry. The binding energies decrease in the order of the three axes a , b , and c . On the other hand, the bonds in the AF phase with $k = 0$ are of tetragonal symmetry. The tetragonal symmetry is also present in the phases with $k = (0,0,k_z)$ and $k = (\frac{1}{2},\frac{1}{2},\frac{1}{2})$. There are different possibilities for the distribution of coexisting magnetic phases in the sample. Phases exist in different volume elements, or some or all superimpose on the same lattice. Powder diffraction does not allow distinguishing these cases. The high sample homogeneity, the temperature homogeneity in the measurements, and the continuous redistribution of the concentrations of different

phases favor a model with one homogeneous antiferromagnetic structure over the entire sample. In the $x(\text{Cu})$ - T phase diagram, the order of appearance of the phases around 25 K between $x(\text{Cu}) = 0$ and 0.12 is $\mathbf{k} = 0 \rightarrow (0, k_y, k_z) \rightarrow (0, 0, k_z) \rightarrow (0, 0, 1)/(\frac{1}{2}, \frac{1}{2}, \frac{1}{2})$. Considering the increasing value of k_z from 0.5 to almost one, one observes a gradual change from a structure with two planes ab and ac with AF bonds towards a structure with an ab plane characterized by AF-bonded spins. For the latter structure both remaining layers can contain a “mixture” of AF and F of different weights between AF and F. This qualitatively correlates with an increasing elongated tetragonal and a decreasing orthorhombic distortion of the crystal lattice.

Canted antiferromagnetism and ferrimagnetism for spinels AB_2O_4 are described in mean-field theory by couplings J_{AA} , J_{AB} , and J_{BB} between different sublattices [31,32]. Moment canting on the Cr^{3+} ions is attributed to the ferrimagnetic J_{AB} exchange. Our measurements show that for samples with higher Cu content than $\text{Ni}_{0.50}\text{Cu}_{0.50}\text{Cr}_2\text{O}_4$, Cr moments canting is present at higher temperature than Ni/Cu order. We conclude that instead of long-range order on the A position, strong short-range correlations of ferrimagnetic nature should be considered to explain the moment canting of Cr. The additional increase in the Cr-AF mode with the onset of

ferromagnetic A order to form ferrimagnetism indicates the relevance of J_{AB} and J_{BB} . The Cr-F mode connects Cu-F and Cr-AF ordering.

The investigation of magnetic structures of samples in the range from $x(\text{Cu})$ from 0 to 0.12 shows a coexistence of commensurate and an incommensurate one of sinusoidal type. Relevant phases have the wave vectors $\mathbf{k} = 0, (0, k_y, k_z), (0, 0, k_z), (0, 0, 1)/(\frac{1}{2}, \frac{1}{2}, \frac{1}{2})$. Structure factors of the Cr tetrahedron show that at least half of the tetrahedra have a uniaxial spin distribution with zero net moment in all phases. Our qualitative analysis indicates that a single magnetic structure, composed of a superposition of different magnetic phases, is consistently embedded in the JT distorted lattice. Changes in a single phase and between single magnetic phases follow the changes in the Ni/Cu ratio of the samples and the thereby induced changes in the JT distortions. The changes in the magnetic system are often delayed compared to the changes in distortion in the crystal. To come to an explanation of this behavior, theoretical investigations are certainly required.

ACKNOWLEDGMENTS

We thank Norbert Stüsser for his valuable contribution to this project. Further, we thank Ralf Feyerherm for critical reading of the manuscript and valuable discussions.

-
- [1] L. Balents, *Nature (London)* **464**, 199 (2010).
- [2] A. P. Ramirez, Geometrical frustration, in *Handbook of Magnetic Materials*, edited by K. H. J. Buschow (North-Holland Elsevier, 2001), Vol. 13, p. 423.
- [3] H. Takagi and S. Niitaka, Highly frustrated magnetism in spinels, in *Introduction to Frustrated Magnetism: Materials, Experiments, Theory*, edited by C. Lacroix, P. Mendels, and F. Mila, Springer Series in Solid State Science Vol. 164 (Springer, Berlin, 2011), p. 155.
- [4] A. N. Yaresko, *Phys. Rev. B* **77**, 115106 (2008).
- [5] S. Ji, S.-H. Lee, C. Broholm, T. Y. Koo, W. Ratcliff, S.-W. Cheong, and P. Zschack, *Phys. Rev. Lett.* **103**, 037201 (2009).
- [6] J. T. Chalker, Geometrically frustrated antiferromagnets: Statistical mechanics and dynamics, in *Introduction to Frustrated Magnetism: Materials, Experiments, Theory*, edited by C. Lacroix, P. Mendels, and F. Mila, Springer Series in Solid State Science Vol. 164 (Springer, Berlin, 2011), p. 3.
- [7] G. F. Dionne, *Magnetic Oxides* (Springer, New York, 2009).
- [8] K. Tomiyasu and I. Kagomiya, *J. Phys. Soc. Jpn.* **73**, 2539 (2004).
- [9] H. Ishibashi and T. Yasumi, *J. Magn. Magn. Mater.* **310**, e610 (2007).
- [10] M. R. Suchomel, D. P. Shoemaker, L. Ribaud, M. C. Kemei, and R. Seshadri, *Phys. Rev. B* **86**, 054406 (2012).
- [11] M. Tovar, R. Torabi, C. Welker, and F. Fleischer, *Physica B* **385**, 196 (2006).
- [12] O. Tchernyshyov, R. Moessner, and S. L. Sondhi, *Phys. Rev. B* **66**, 064403 (2002).
- [13] A. Chatterjee, J. K. Dey, S. Majumdar, A.-C. Dippel, O. Gutowski, M. v. Zimmermann, and S. Giri, *Phys. Rev. Mater.* **3**, 104403 (2019).
- [14] Y. Yamasaki, S. Miyasaka, Y. Kaneko, J.-P. He, T. Arima, and Y. Tokura, *Phys. Rev. Lett.* **96**, 207204 (2006).
- [15] R. Borah and S. Ravi, *J. Magn. Magn. Mater.* **502**, 166550 (2020).
- [16] S. C. Tarantino, M. Giannini, M. A. Carpenter, and M. Zema, *IUCrJ* **3**, 354 (2016).
- [17] A. Das, R. Pal, S. Mehta, K. P. Islam, A. Mondal, A. N. Pal, and D. Choudhury, *Phys. Rev. B* **109**, 024104 (2024).
- [18] N. Menyuk, K. Dwight, and A. Wold, *J. Phys. (Paris)* **25**, 528 (1964).
- [19] K. Tomiyasu, J. Fukunaga, and H. Suzuki, *Phys. Rev. B* **70**, 214434 (2004).
- [20] M. Reehuis, M. Tovar, D. M. Többens, P. Pattison, A. Hoser, and B. Lake, *Phys. Rev. B* **91**, 024407 (2015).
- [21] N. Stüsser, M. Reehuis, M. Tovar, B. Klemke, A. Hoser, and J.-U. Hoffmann, *Phys. Rev. B* **98**, 144424 (2018).
- [22] N. Stüsser, M. Reehuis, M. Tovar, B. Klemke, A. Hoser, and J.-U. Hoffmann, *J. Magn. Magn. Mater.* **506**, 166683 (2020).
- [23] D. M. Többens and S. Zander, *J. Large-Scale Res. Fac.* **2**, A49 (2016).
- [24] D. Wallacher, N. Grimm, and V. Bon, https://www.helmholtz-berlin.de/pubbin/igama_output?modus=einzel&sprache=en&gid=2130&typoid=76061.
- [25] J.-U. Hoffmann and M. Reehuis, *J. Large-Scale Res. Fac.* **4**, A129 (2018).
- [26] J. Rodriguez-Carvajal, *Physica B* **192**, 55 (1993).
- [27] E. F. Bertaut and J. Dulac, *Acta Crystallogr. A* **28**, 580 (1972).
- [28] R. J. Elliott, *Phys. Rev.* **124**, 346 (1961).
- [29] M. Kataoka and J. Kanamori, *J. Phys. Soc. Jpn.* **32**, 113 (1972).
- [30] M. P. Ivliev, A. A. Mukovnin, V. P. Sakhnenko, and V. M. Talanov, *Phys. Solid State* **56**, 2077 (2014).
- [31] Y. Yafet and C. Kittel, *Phys. Rev.* **87**, 290 (1952).
- [32] H. Kaplan, *Phys. Rev.* **86**, 121 (1952).